

## Contact analysis using Trefftz and interface finite elements

Ke Y. Wang, Manicka Dhanasekar

*Centre for Railway Engineering, Central Queensland University, QLD 4702, Australia*

Qing H. Qin

*Department of Engineering, Australian National University, ACT0200, Australia*

Yi L. Kang

*Department of Mechanics*

*Tianjin University, 300072, PR China*

(Received March 17, 2006)

Hybrid-Trefftz (HT) finite element (FE) analysis of two-dimensional elastic contact problems is addressed with the aid of interface elements and an interfacial constitutive relation. This paper presents the formulation of a four-noded HT finite element for discretizing the contacting bodies and a four-noded interface element that could be embedded in the prospective contact zone for simulating the interaction behaviour. Due to the superior performance, the Simpson-type Newton–Cotes integration scheme is utilized to compute interface element formulation numerically. In order to evaluate the applicability of the present approach two benchmark examples are investigated in detail. Comparisons have been made between the results by the present approach and analytical as well as traditional FE solutions using ABAQUS software.

### 1. INTRODUCTION

Contact problems have attracted much attention due to their inherent complexity and frequent occurrence in engineering practice. A variety of numerical approaches for calculating contact zones, and dividing them into stick and slip subzones, as well as determining the contact stresses, are available in the literature. Amongst these approaches the interface element (IE) methodology, due to its ease of numerical implementation, has been investigated by many researchers. Goodman *et al.* [5] presented the pioneering work on such an element for evaluating the behaviour of jointed rock mass. However, the kinematic inconsistency associated with this element usually has resulted in spurious oscillations of tangential traction. To circumvent this difficulty, the Newton–Cotes integration scheme was used by several authors instead of the widely adopted Gaussian quadrature [2, 16, 24]. Day and Potts [2] argued that the reduced Gauss integration used by Gens *et al.* [4] could not avoid the oscillation of the traction profile. Lei [16] illustrated the performance of Newton–Cotes integration scheme through two examples of a smooth footing on elastic sub-soil and a pull-out problem. Schellekens and De Borst [24] specially discussed this integration scheme and provided an explanation for some numerical results. They pointed out that, for either linear or quadratic interface elements, the aforementioned oscillations can not be recovered in the case of high gradient tractions. Therefore, other types [7, 14] of interface element were subsequently proposed in the literature. Herrmann [7] assumed each pair of matching nodes has been linked through fictitious springs - one normal and the other tangential to the interface. Although such treatment overcomes the disadvantage occurring in Goodman-type element, the uncoupling between links does not accord totally with the practice and often leads to unreliable normal response. In the light of this, Kalkan and Li [14] have developed an improved type of element which possesses the normal response

characteristics of the Goodman element, and eliminates the kinematic deficiencies by employing tangential response similar to the Herrmann element [7].

As a promising technique for the numerical solution of a variety of problems encountered in engineering, HT FE approach assimilates the merits of the conventional FE and boundary element (BE) methods and, moreover, discards some of their drawbacks [19]: Firstly, the element formulation calls for integration along the element boundaries only, and secondly, some problems with singular or local effects can be treated easily if exact local solution functions are available. A general purpose HT FE formulation was first developed by Jirousek and Leon [10] who studied the effect of mesh distortion on thin plate elements. Since then, the HT element concept has become increasingly popular, attracting a growing number of researchers into this field [19]. So far, HT elements have been successfully applied to numerous problems such as elasticity [12, 13], elastoplasticity [3, 23], plates [9, 18], transient heat conduction analysis [11] and piezoelectric materials [20, 21]. According to authors' knowledge, there are only a few papers [8, 27] reporting application of HT FE technique to contact problems in the literature. Hochard [8] dealt with frictionless contact between an elastic domain and a rigid support by transforming the equations of contact to a problem of minimization under linear constraints. Recently, Wang *et al.* [27] developed a HT FE interface model for contact problems with the aid of direct constraint approach.

The purpose of this paper is to develop a HT FE model and apply it to elastic contact problems with the help of Kaliakin–Li (KL) interface elements [14]. In the model, a 4-node HT element has been formulated and applied for discretizing both contacting bodies; 4-node KL elements have been embedded for simulating the potential contact zone. To assess the reliability of the KL elements for predicting the contact behaviour, an interfacial constitutive relation, namely penalised normal contact and tangential friction law, has been adopted. In addition, the Simpson-type Newton–Cotes integration scheme [6] is recommended to evaluate the formulation of the KL element in this analysis. Two benchmark examples have been presented to illustrate the applicability of the overall model to contact problems. Good agreements have been achieved between the results from the present approach and analytical as well as the conventional FE solutions obtained from ABAQUS software.

This paper illustrates how to construct the contact model via ABAQUS user element subroutine UEL. Applications show that this approach can save more time on UEL than on programming the whole in-house FE code. Therefore, it may be a promising way to the analysis of practical engineering problems.

## 2. HYBRID TREFFTZ AND INTERFACE ELEMENT MODEL

### 2.1. HT element formulation

Figure 1 shows two linear elastic bodies  $\Omega^A$  and  $\Omega^B$  in closer contact. The boundary  $\Gamma^\alpha$  of each body  $\Omega^\alpha$  ( $\alpha = A, B$ ) consists of three disjointed portions  $\Gamma_u^\alpha = \Gamma_t^\alpha$  and  $\Gamma_c^\alpha$ .  $\Gamma_u^\alpha$  and  $\Gamma_t^\alpha$  are prescribed displacement and traction boundaries respectively,  $\Gamma_c^\alpha$  represents the prospective contact surface of each body which should be assumed large enough to contain the actual contact surface after deformation. The basic equations of HT FE model in the global Cartesian coordinates  $X_i$  ( $i = 1, 2$ ) are summarized as follows,

$$\sigma_{ij,j} + \bar{b}_i = 0 \quad \text{in } \Omega^A \cup \Omega^B, \quad (1a)$$

$$\left. \begin{aligned} \sigma_{ij} &= D_{ijkl}\varepsilon_{kl} \\ \varepsilon_{ij} &= C_{ijkl}\sigma_{kl} \\ \varepsilon_{ij} &= \frac{1}{2}(u_{i,j} + u_{j,i}) \end{aligned} \right\} \quad \text{in } \Omega^A \cup \Omega^B, \quad (1b)$$

$$u_i = \bar{u}_i \quad \text{on } \Gamma_u^A \cup \Gamma_u^B, \quad (1c)$$

$$t_i = \sigma_{ij}n_j = \bar{t}_i \quad \text{on } \Gamma_t^A \cup \Gamma_t^B, \quad (1d)$$

$$u_{ia} = u_{ib} \quad \text{on } \Gamma_a \cap \Gamma_b, \quad (1e)$$

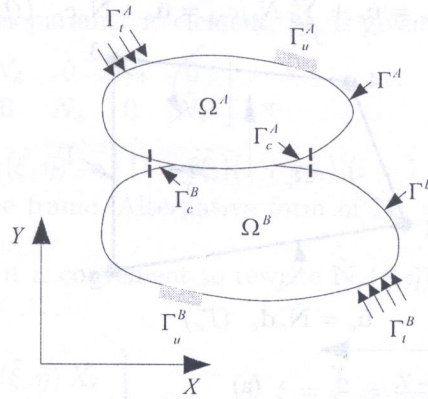


Fig. 1. Graphic representation of contact problem

$$t_{ia} + t_{ib} = 0 \quad \text{on } \Gamma_a \cap \Gamma_b, \tag{1f}$$

Equations (1a–d) are the fundamental relations of conventional FEM, while Eqs. (1e–f) are additional inter-element continuity requirements for HT FEM.  $\sigma_{ij}$  and  $\varepsilon_{ij}$  are respectively the stress and strain tensors,  $D_{ijkl}$  and  $C_{ijkl}$  – the stiffness and compliance coefficient tensors,  $u_i$ ,  $t_i$  and  $b_i$  denote respectively displacements, tractions and body forces and overhead bar stands for prescribed value,  $n_j$  stand for direction cosines of the outward normal at a given point on the boundary, subscripts “a” and “b” represent any two adjacent elements.

To establish the formulation for a particular HT element “e”, two groups of distinct displacement fields [13] (see Fig. 2):

- (i) a nonconforming intra-element displacement field (Trefftz field)

$$\mathbf{u}_e = \bar{\mathbf{u}}_e + \sum_{j=1}^m N_{ej} \mathbf{c}_{ej} = \bar{\mathbf{u}}_e + \mathbf{N}_e \mathbf{c}_e \quad \text{in } \Omega_e, \tag{2a}$$

- (ii) an exactly and minimally conforming auxiliary frame field

$$\tilde{\mathbf{u}}_e = \tilde{\mathbf{N}}_e \mathbf{d}_e \quad \text{on } \Gamma_e, \tag{2b}$$

are assumed on the basis of the Trefftz method. Where  $\bar{\mathbf{u}}_e$  and  $\mathbf{N}_e$  are, respectively, the particular and homogeneous solutions (so-called Trefftz functions) to Eq. (1a),  $\mathbf{c}_e$  is a vector of unknown parameters,  $m$  is the number of Trefftz solutions,  $\tilde{\mathbf{N}}_e$  are the shape functions (frame functions) defined in the customary way, the tilde appearing in Eq. (2b) indicates that the frame field is defined on the element boundary only.

A complete system of Trefftz functions  $\mathbf{N}_e$  may be generated with the aid of Muskhelishvili’s of complex variable formulation. The results presented in [13] are listed in Appendix A. It is important to determine the optimal value of  $m$  with respect to accuracy and computational effort in HT FE analysis. Wang *et al.* [27] stated that the choice of  $m = 9$  can produce robust 4-node plane HT element so that

$$\mathbf{N}_e = \mathbf{N}_e(x, y) = \frac{1}{2G} \begin{bmatrix} (\kappa - 1)x & y & -x & -2\kappa xy & (\kappa - 2)x^2 - (\kappa + 2)y^2 \\ (\kappa - 1)y & x & y & (\kappa + 2)x^2 - (\kappa - 2)y^2 & 2\kappa xy \\ 2xy & y^2 - x^2 & (3 - 3\kappa)x^2 y + (\kappa + 3)y^3 & (\kappa - 3)x^3 - (3\kappa + 3)xy^2 \\ x^2 - y^2 & 2xy & (\kappa + 3)x^3 - (3\kappa - 3)xy^2 & (3\kappa + 3)x^2 y - (\kappa - 3)y^3 \end{bmatrix} \tag{3}$$

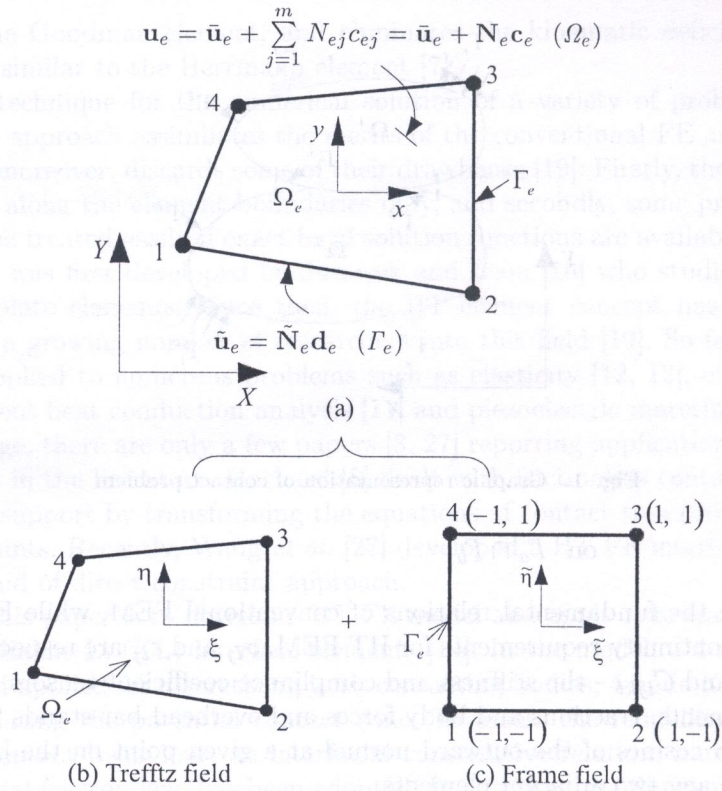


Fig. 2. Four-noded HT element

where  $G = E/(2 + 2\nu)$ ,  $\kappa = 3 - 4\nu$  for plane stress whereas  $\kappa = (3 - 7\nu)/(1 - \nu)$  for plane strain,  $E$  and  $\nu$  are respectively Young's modulus and Poisson's ratio and  $(x, y)$  is the local Cartesian coordinate system which originates at the element centroid

$$\begin{cases} x = X - X_0 = X - \frac{1}{4} \sum_{i=1}^4 X_i \\ y = Y - Y_0 = Y - \frac{1}{4} \sum_{i=1}^4 Y_i \end{cases} \quad (4)$$

where  $X_0, Y_0$  and  $X_i, Y_i$  are, respectively, the global Cartesian coordinates of centroid and nodes of the element. In HT FE implementation, additionally, a so-called Trefftz dimensionless coordinate system  $(\xi, \eta)$ ,

$$\xi = \frac{x}{l_e}, \quad \eta = \frac{y}{l_e}, \quad (5)$$

together with

$$l_e = \frac{1}{4} \sum_{i=1}^4 \sqrt{x_i^2 + y_i^2}, \quad (6)$$

has to be used to ensure a good numerical conditioning of the element flexibility matrix  $\mathbf{H}_e$  defined below. Where  $l_e$  denotes the average distance between the element nodes and its centroid (termed element characteristic length). In practice, replacing  $x$  and  $y$  in Eq.(3) by  $\xi$  and  $\eta$  and extracting  $l_e$  produces

$$\mathbf{N}_e = \mathbf{N}_e(x, y) = \mathbf{N}_e(\xi, \eta) \mathbf{L}_e(l_e) \quad (7)$$

where  $\mathbf{L}_e(l_e)$  is a diagonal matrix with respect to the element characteristic length; for  $m = 9$ ,  $\mathbf{L}_e(l_e) = \text{diag}(l_e \ l_e \ l_e \ l_e^2 \ l_e^2 \ l_e^2 \ l_e^2 \ l_e^3 \ l_e^3)$ .

According to the concept of isoparametric element,  $\tilde{\mathbf{N}}_e$  is given as

$$\tilde{\mathbf{N}}_e = \begin{bmatrix} \tilde{N}_1 & 0 & \tilde{N}_2 & 0 & \tilde{N}_3 & 0 & \tilde{N}_4 & 0 \\ 0 & \tilde{N}_1 & 0 & \tilde{N}_2 & 0 & \tilde{N}_3 & 0 & \tilde{N}_4 \end{bmatrix} \quad (8)$$

for 4-node HT element. Here,  $\tilde{N}_i(\tilde{\xi}, \tilde{\eta}) = \frac{1}{4} (1 + \tilde{\xi}\tilde{\xi}_i)(1 + \tilde{\eta}\tilde{\eta}_i)$  ( $i = 1, 2, 3, 4$ ),  $(\tilde{\xi}, \tilde{\eta})$  stands for isoparametric coordinate system for the frame. Alternative form of  $\tilde{\mathbf{N}}_e$  which is equivalent to Eq. (8) is used by Qin [19].

For numerical computations, it is convenient to rewrite  $\tilde{\mathbf{N}}_e(\tilde{\xi}, \tilde{\eta})$  in terms of  $\xi$  and  $\eta$  by a simple relation [26]

$$\begin{Bmatrix} \tilde{\xi} \\ \tilde{\eta} \end{Bmatrix} \Rightarrow \begin{Bmatrix} X = \sum_{i=1}^4 \tilde{N}_i(\tilde{\xi}, \tilde{\eta}) X_i \\ Y = \sum_{i=1}^4 \tilde{N}_i(\tilde{\xi}, \tilde{\eta}) Y_i \end{Bmatrix} \Rightarrow \begin{Bmatrix} \xi = \frac{x}{l_e} = \frac{X-X_0}{l_e} \\ \eta = \frac{y}{l_e} = \frac{Y-Y_0}{l_e} \end{Bmatrix} \quad (9)$$

and then

$$\tilde{\mathbf{N}}_e = \tilde{\mathbf{N}}_e(\tilde{\xi}, \tilde{\eta}) = \tilde{\mathbf{N}}_e(x, y) = \tilde{\mathbf{N}}_e(\xi, \eta) \quad (10)$$

The corresponding traction field  $\mathbf{t}_e$  can be derived from Eqs. (1b,d) and (2a) such that

$$\mathbf{t}_e = \bar{\mathbf{t}}_e + \sum_{j=1}^m Q_{ej} \mathbf{c}_j = \bar{\mathbf{t}}_e + \mathbf{Q}_e \mathbf{c}_e \quad (11)$$

where  $\mathbf{Q}_e = \mathbf{A} \mathbf{D} \mathbf{L} \mathbf{N}_e$ , in which  $\mathbf{A}$ ,  $\mathbf{D}$  and  $\mathbf{L}$  are transformation, constitutive and differential operator matrices, respectively [19].

According to the modified variational principles presented by Qin [22]

$$\Pi_m = \sum_e \Pi_{me} = \sum_e \left[ \Pi_e - \int_{\Gamma_{et}} (t_i - \bar{t}_i) \tilde{u}_i \, d\Gamma - \int_{\Gamma_{eI}} t_i \tilde{u}_i \, d\Gamma \right], \quad (12a)$$

$$\Psi_m = \sum_e \Psi_{me} = \sum_e \left[ \Psi_e - \int_{\Gamma_{eu}} (u_i - \bar{u}_i) t_i \, d\Gamma - \int_{\Gamma_{eI}} t_i \tilde{u}_i \, d\Gamma \right], \quad (12b)$$

where  $\Pi_e$  and  $\Psi_e$  are, respectively, the minimum potential and complementary functionals,  $\Gamma_e = \Gamma_{eu} \cup \Gamma_{et} \cup \Gamma_{eI}$ , while  $\Gamma_{eu} = \Gamma_u \cap \Gamma_e$ ,  $\Gamma_{et} = \Gamma_t \cap \Gamma_e$ , and  $\Gamma_{eI}$  is the inter-element boundary of element "e".

Taking the vanishing variation of Eq. (12a) or (12b) we can readily obtain the customary force-displacement relationship, i.e. the element stiffness equation as

$$\mathbf{K}_e \mathbf{d}_e = \mathbf{P}_e \quad (13)$$

where

$$\mathbf{K}_e = \mathbf{G}_e^T \mathbf{H}_e^{-1} \mathbf{G}_e, \quad (14a)$$

$$\mathbf{P}_e = \mathbf{G}_e^T \mathbf{H}_e^{-1} \mathbf{h}_e + \mathbf{g}_e. \quad (14b)$$

The derivation of the element stiffness equation from Eq. (12a) and the expressions for auxiliary matrices  $\mathbf{H}_e$ ,  $\mathbf{G}_e$ ,  $\mathbf{h}_e$  and  $\mathbf{g}_e$  can be found in [22].

By using Eqs. (7) and (10) and making some manipulation, we obtain the following expressions of  $\mathbf{K}_e$  and  $\mathbf{P}_e$ ,

$$\mathbf{K}_e = \mathbf{K}_e(x, y) = \mathbf{K}_e(\xi, \eta), \quad (15a)$$

$$\mathbf{P}_e = \mathbf{P}_e(x, y) = \mathbf{P}_e(\xi, \eta). \quad (15b)$$

It is obviously noted that  $\mathbf{K}_e$  and  $\mathbf{P}_e$  remain truly unchanged in their magnitude from the local Cartesian coordinate system to the Trefftz dimensionless one. Therefore, we can use the right hand side of Eqs. (15a,b) to evaluate the HT element stiffness equation directly.

### 2.2. KL interface element formulation

KL interface element not only possesses the normal response characteristics of Goodman-type element but also eliminates the kinematic inconsistencies of the tangential response by employing the logic of Herrmann-type element [14]. Since our paper focuses on the application of HT and KL elements through UEL to contact problems rather than on KL interface element itself, the formulation of KL element is briefly reviewed. A representative 4-node KL interface element is depicted in Fig. 3. Such element possesses zero thickness before deformation.

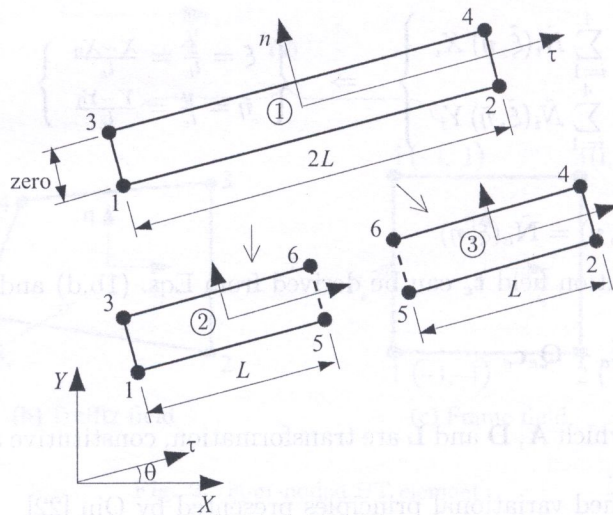


Fig. 3. Four-noded KL interface element

In order to derive the element formulation KL element 1-2-3-4 (denoted by ①) is decomposed into two sub elements 1-5-3-6 (denoted by ②) and 5-2-6-4 (denoted by ③) in Fig. 3. Adopting the idea of Goodman *et al.* [5], the relative displacement vector,  $\hat{\mathbf{w}} = \{ \hat{w}_\tau \hat{w}_n \}^T$ , at any generic point of interface with respect to the local system  $(\tau, n)$  may be defined as

$$\hat{\mathbf{w}} = \begin{Bmatrix} \hat{w}_\tau \\ \hat{w}_n \end{Bmatrix} = \begin{Bmatrix} u_\tau^{\text{top}} - u_\tau^{\text{bot}} \\ u_n^{\text{top}} - u_n^{\text{bot}} \end{Bmatrix} = \Phi \hat{\mathbf{d}}'_e \tag{16}$$

where

$$\Phi = -\mathbf{M} : \mathbf{M} \quad \text{with} \quad \mathbf{M} = \begin{bmatrix} m_1 & 0 & m_2 & 0 \\ 0 & m_1 & 0 & m_2 \end{bmatrix} \tag{17a}$$

$$\hat{\mathbf{d}}'_e = \{ u_{1\tau} \ u_{1n} \ u_{2\tau} \ u_{2n} \ u_{3\tau} \ u_{3n} \ u_{4\tau} \ u_{4n} \}^T \tag{17b}$$

in which  $m_1 = \frac{1}{2}(1 - \zeta)$ ,  $m_2 = \frac{1}{2}(1 + \zeta)$ , the superscript  $\hat{\cdot}$  stands for variables of the interface.

Accordingly, the traction vector,  $\hat{\boldsymbol{\sigma}} = \{ \hat{\sigma}_\tau \ \hat{\sigma}_n \}^T$ , is readily expressed as

$$\hat{\boldsymbol{\sigma}} = \mathbf{D} \hat{\mathbf{w}} = \mathbf{D} \Phi \hat{\mathbf{d}}'_e \tag{18}$$

where  $\mathbf{D} = \text{diag}(k_\tau \ k_n)$  is the interfacial constitutive matrix,  $k_\tau$  and  $k_n$  are, respectively, the tangential and normal penalty stiffness parameters of the interface.

By using the virtual work principle, the stiffness equation of the Goodman-type element in the local system is defined as

$$*\hat{\mathbf{K}}'_e * \hat{\mathbf{d}}'_e = *\hat{\mathbf{P}}'_e \tag{19}$$

together with

$$*\hat{\mathbf{K}}'_e = \frac{L}{2} \int_{-1}^{+1} \Phi^T \mathbf{D} \Phi \, d\zeta, \tag{20a}$$

$$*\hat{\mathbf{P}}'_e = \frac{L}{2} \int_{-1}^{+1} \Phi^T \hat{\boldsymbol{\sigma}} \, d\zeta, \tag{20b}$$

$$*\hat{\mathbf{d}}'_e = \text{from Eq. (17b)}. \tag{20c}$$

It is worth noting that the integrals appearing in above equation are performed by the Simpson-type of the Newton–Cotes integration scheme [6]. Next, using standard assembly procedure the stiffness equations of elements ② and ③ can be combined into a form

$$**\hat{\mathbf{K}}'_e **\hat{\mathbf{d}}'_e = **\hat{\mathbf{P}}'_e \tag{21}$$

where

$$**\hat{\mathbf{d}}'_e = \{ u_{1\tau} \ u_{1n} \ u_{2\tau} \ u_{2n} \ u_{3\tau} \ u_{3n} \ u_{4\tau} \ u_{4n} \ u_{5\tau} \ u_{5n} \ u_{6\tau} \ u_{6n} \}^T. \tag{22}$$

Equation (21) can also be written in terms of submatrices as

$$\begin{bmatrix} \hat{\mathbf{K}}_{rr} & \hat{\mathbf{K}}_{rc} \\ \hat{\mathbf{K}}_{cr} & \hat{\mathbf{K}}_{cc} \end{bmatrix} \begin{Bmatrix} \hat{\mathbf{d}}_r \\ \hat{\mathbf{d}}_c \end{Bmatrix} = \begin{Bmatrix} \hat{\mathbf{P}}_r \\ \hat{\mathbf{P}}_c \end{Bmatrix} \tag{23}$$

where subscript *c* stands for variables associated with nodes 5 and 6 whilst *r* with nodes 1, 2, 3 and 4.

The solution of the second submatrix equation of Eq. (23) for  $\hat{\mathbf{d}}_c$  yields

$$\hat{\mathbf{d}}_c = \hat{\mathbf{K}}_{cc}^{-1} \left( \hat{\mathbf{P}}_c - \hat{\mathbf{K}}_{cr} \hat{\mathbf{d}}_r \right). \tag{24}$$

Substituting Eq. (24) into the first submatrix equation of Eq. (23) to eliminate  $\hat{\mathbf{d}}_c$  leads to

$$\hat{\mathbf{K}}'_e \hat{\mathbf{d}}'_e = \hat{\mathbf{P}}'_e \tag{25}$$

where

$$\hat{\mathbf{K}}'_e = \hat{\mathbf{K}}_{rr} - \hat{\mathbf{K}}_{rc} \hat{\mathbf{K}}_{cc}^{-1} \hat{\mathbf{K}}_{cr}^T, \tag{26a}$$

$$\hat{\mathbf{P}}'_e = \hat{\mathbf{P}}_r - \hat{\mathbf{K}}_{rc} \hat{\mathbf{K}}_{cc}^{-1} \hat{\mathbf{P}}_c. \tag{26b}$$

The elimination process from Eq. (23) to Eq. (25) is completed by static condensation [28]. Here,  $\hat{\mathbf{K}}'_e$  and  $\hat{\mathbf{P}}'_e$  are, respectively, the equivalent stiffness matrix and nodal force vector of KL interface element.

For solution purpose, the KL element stiffness equation (25) must be transformed into the form in the global Cartesian coordinate system (*X*, *Y*) so that

$$\hat{\mathbf{K}}_e \hat{\mathbf{d}}_e = \hat{\mathbf{P}}_e \tag{27}$$

together with

$$\hat{\mathbf{K}}_e = [\mathbf{R}^*]^T \hat{\mathbf{K}}'_e \mathbf{R}^*, \tag{28a}$$

$$\hat{\mathbf{P}}_e = [\mathbf{R}^*]^T \hat{\mathbf{P}}'_e, \tag{28b}$$

$$\hat{\mathbf{d}}_e = \{ u_{1X} \ u_{1Y} \ u_{2X} \ u_{2Y} \ u_{3X} \ u_{3Y} \ u_{4X} \ u_{4Y} \}^T \tag{28c}$$

in which

$$\mathbf{R}^* = \text{diag}[\mathbf{R} \ \mathbf{R} \ \mathbf{R} \ \mathbf{R}] \quad \text{with} \quad \mathbf{R} = \begin{Bmatrix} \cos \theta & \sin \theta \\ -\sin \theta & \cos \theta \end{Bmatrix}. \tag{29}$$

### 2.3. Interface model and numerical implementation

Figure 4 shows a contact interface model, where a prospective contact zone  $\Omega^C$  may be bounded by the boundaries  $\Gamma_c^A, \Gamma_c^B, \Gamma_1$  and  $\Gamma_2$ . 4-node KL interface elements are embedded in the prospective contact zone for simulating the behaviour of interaction.

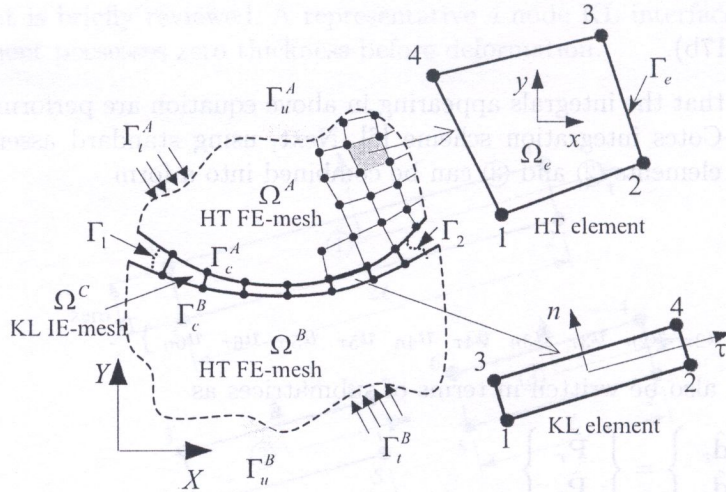


Fig. 4. Two HT element subdomains in contact with KL elements

In order to evaluate contact non-linearity, an appropriately interfacial constitutive relation, namely normal and tangential stress-relative displacement curves, is established for the KL element (see Fig. 5). In accordance with Fig. 4, the corresponding stresses  $\sigma_\tau, \sigma_n$  in Eq. (18) can be rewritten as follows,

$$\sigma_n = \begin{cases} 0 & \text{if } w_n > 0 \\ k_n w_n & \text{otherwise} \end{cases} \quad \begin{matrix} \text{separation} \\ \text{contact} \end{matrix} \quad (30a)$$

$$\sigma_\tau = \begin{cases} 0 & \text{if } w_n > 0 \\ k_\tau w_\tau & \text{if } w_n \leq 0 \text{ and } |w_\tau| \leq -\mu \frac{k_n}{k_\tau} w_n \\ -\mu k_n w_n & \text{if } w_n \leq 0 \text{ and } |w_\tau| > -\mu \frac{k_n}{k_\tau} w_n \end{cases} \quad \begin{matrix} \text{separation} \\ \text{stick} \\ \text{slip} \end{matrix} \quad (30b)$$

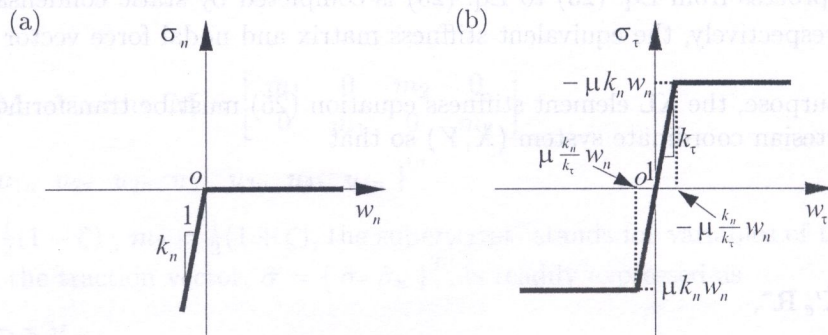


Fig. 5. Schematic representation of interfacial constitutive relation; (a) normal direction, (b) tangential direction

For clarity, the algorithm is described as follows:

Step 1: Assume all integration points of current KL element are in stick status and set  $k_n$  and  $k_\tau$



Step 2: Check for  $w_n$  and  $w_\tau$  for every integration point of current KL element and determine what status occurs

IF  $w_n > 0$  (separation) THEN

Set  $k_n = k_\tau = 0$ , compute  $\sigma_n = \sigma_\tau = 0$

ELSE

Compute  $\sigma_n = k_n w_n$ .

IF  $|w_\tau| \leq -\mu \frac{k_n}{k_\tau} w_n$  (stick) THEN

Keep  $k_n$  and  $k_\tau$  unchanged, compute  $\sigma_\tau = k_\tau w_\tau$

ELSE (slip)

Keep  $k_n$  unchanged and set  $k_\tau = 0$ , compute  $\sigma_\tau = -\mu k_n w_n$

END IF

END IF

Step 3: Output the contact pressures and shear stresses.

It is clear from Eq. (30b) that the classical Coulomb friction law is considered for tangential behaviour of the interface. In addition, special attention must be paid to the choice of the optimum values of penalty parameters  $k_\tau$ ,  $k_n$ . Excessively high values tend to provide ill-conditioned numerical problem whilst too small values could not prevent the penetration between the two contacting bodies. Although automatic calculations of the penalty parameters have been reported in the literature [1, 17], these approaches have some limitations, such as not taking into account of the separation mode or frictional effects across the interface in the analysis. Therefore, in the next section a parametric study on  $k_\tau$ ,  $k_n$  will be carried out in detail through numerical examples.

The HT FE-interface model for contact problems has been implemented in ABAQUS via user element subroutine (UEL) including both HT and KL elements. The iterations for calculating the stresses of Eqs. (30a,b) at the interface are completed within the UEL.

### 3. NUMERICAL EXAMPLES

In order to assess the HT FE-interface contact model developed in this paper, two benchmark examples were considered. The assumption of plane strain condition was made in the subsequent analyses. It should be noted that all results obtained from ABAQUS are based on the contact property options: "hard" contact pressure-overclosure and penalty friction formulation.

#### Example 1. A block resting on a substratum

As shown in Fig. 6, a block is pressed on a substratum with the pressure of  $q = 100$  MPa on its top surface. The geometry and boundary conditions are also shown in the figure. Material properties of both bodies are the same with Young's moduli  $E^A = E^B = 2000$  MPa and Poisson's ratios  $\nu^A = \nu^B = 0.3$ .

Three different meshes used in the analyses are illustrated in Fig. 7. Fine mesh was uniformly used in the vicinity of singularity point  $P$  and potential stick-slip boundary. Table 1 shows the mesh properties, the CPU time and convergence of displacements and shear stress at point  $P$ . Since the interface penalty stiffnesses  $k_\tau$  and  $k_n$  play a significant role in the numerical analysis, their influence on the contact behaviour was first examined.

Figure 8 shows the penetrations of the KL elements along the interface for a wide range of the ratio of normal stiffness to Young's modulus ( $\frac{k_n}{E_{\max}}$ ) in the frictionless case, where  $E_{\max} = \max(E^A, E^B)$ .

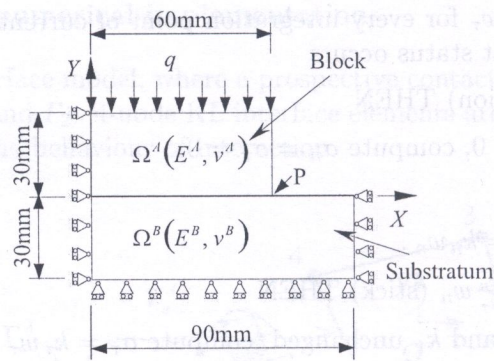


Fig. 6. A block resting on a substratum

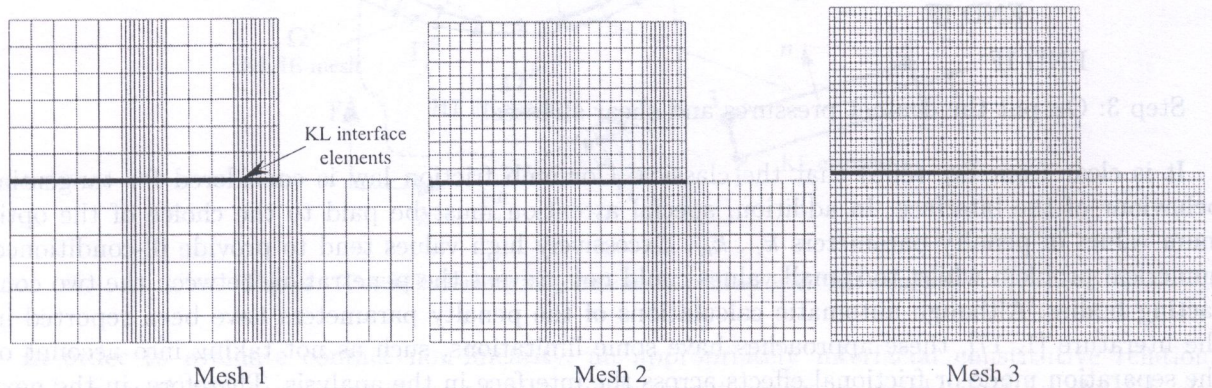


Fig. 7. Mesh convergence studies

Table 1. Mesh properties, CPU time and convergence for Example 1

Mesh	No. of Elements		CPU time (s)		Horizontal Disp. (mm)		Vertical Disp. (mm)		Shear Stress (MPa)	
	HT	KL	Abaqus	Present	Abaqus	Present	Abaqus	Present	Abaqus	Present
1	396	28	21	20	0.835	0.836	-0.685	-0.682	36.466	35.452
2	1044	36	25	23	0.816	0.814	-0.689	-0.687	31.075	30.764
3	3096	52	35	33	0.806	0.810	-0.692	-0.695	28.715	28.077

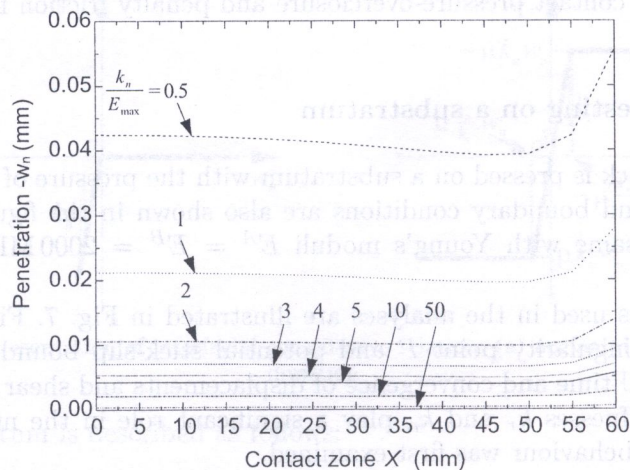


Fig. 8. Effect of  $k_n$  on the penetration in the frictionless case

It can be observed that as the ratio  $\frac{k_n}{E_{\max}}$  increases from 0.5 ~ 50 the penetration decreases. To search an appropriate value of  $k_n$ , an error norm was defined as follows,

$$\text{Error} = \max \left( \frac{w_n}{u_n^{\text{top}}}, \frac{w_n}{u_n^{\text{bot}}} \right)_{\text{sp}} \times 100\%, \tag{31}$$

where the subscript “sp” stands for the sampling (or herein Simpson) points.

From Fig. 9, it can be seen that for  $\frac{k_n}{E_{\max}} \geq 3$  the maximum error has remained less than 2% which is acceptable for most practical applications. Therefore, a reasonable choice for  $k_n$  may be postulated as

$$k_n = (3 \sim 5) E_{\max}. \tag{32}$$

Note that Eq. (32) is just an equality in magnitude or an empirical relationship, the unit of the coefficient is  $\text{mm}^{-1}$ . In this paper we have chosen the relation  $k_n = 5E_{\max}$  for all the analyses.

Next a frictional case with a frictional coefficient  $\mu = 0.1$ , as illustrated in Fig. 10, was considered. The penalty normal stiffness was chosen as  $k_n = 10^4 \text{ N/mm}^3$  whilst three penalty tangential

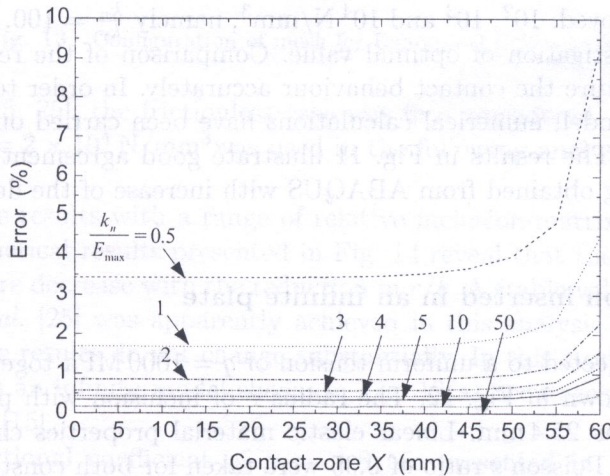


Fig. 9. Error of penetration for different  $k_n$  in the frictionless case

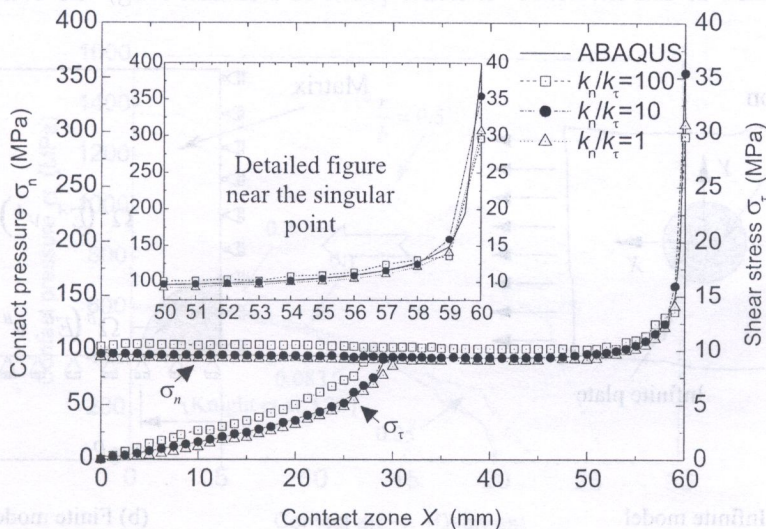


Fig. 10. Effect of interface stiffnesses on the contact behaviour ( $\mu = 0.1$ )

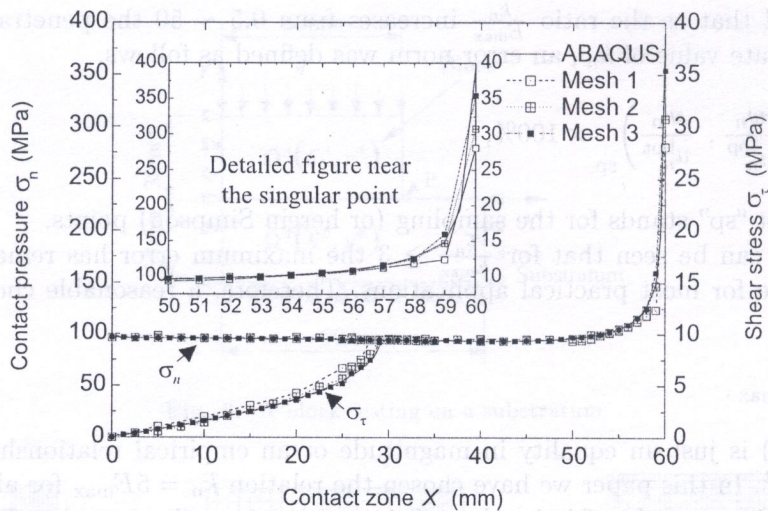


Fig. 11. Convergence study of different meshes ( $k_n/k_\tau = 10$ ;  $\mu = 0.1$ )

stiffnesses of  $k_\tau$  were employed:  $10^2$ ,  $10^3$  and  $10^4$  N/mm<sup>3</sup>, namely  $\frac{k_n}{k_\tau} = 100$ , 10 and 1 in the HT FE-interface analysis for investigation of optimal value. Comparison of the results indicates that the choice of  $\frac{k_n}{k_\tau} = 10$  can capture the contact behaviour accurately. In order to verify the convergence of the HT FE-interface model, numerical calculations have been carried out with different meshes (see Fig. 7) for  $\frac{k_n}{k_\tau} = 10$ . The results in Fig. 11 illustrate good agreement with the results of the conventional FE modelling obtained from ABAQUS with increase of the density of mesh.

**Example 2. An inclusion inserted in an infinite plate**

An inclusion problem subjected to a uniform tension of  $q = 1000$  MPa together with geometry and boundary conditions is shown in Fig. 12. The radius  $r$  of inclusion with perfect fit to the hole of an infinite plate was set as 25.4 mm. Linear elastic material properties characterized by Young’s modulus of 4000 MPa and Poisson’s ratio of 0.35 were taken for both constituent bodies.

For numerical purpose a simplified finite element model was employed (see Fig. 12(b)). Due to symmetry, only a quarter of the problem has been discretised. The simplified model consisted of 8231 HT elements and 40 KL interface elements (each of 0.52 mm long). To conform to the results

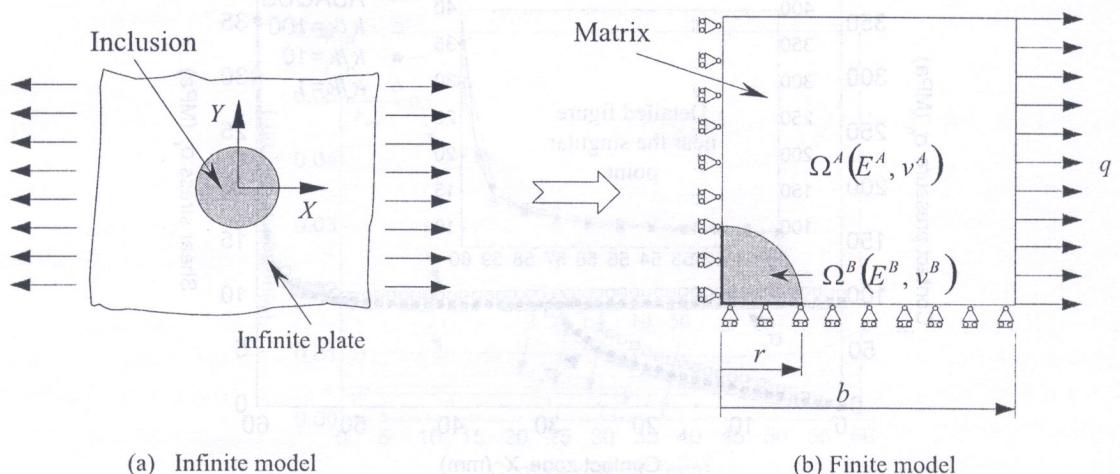


Fig. 12. An inclusion inserted in an infinite plate and its simplified model

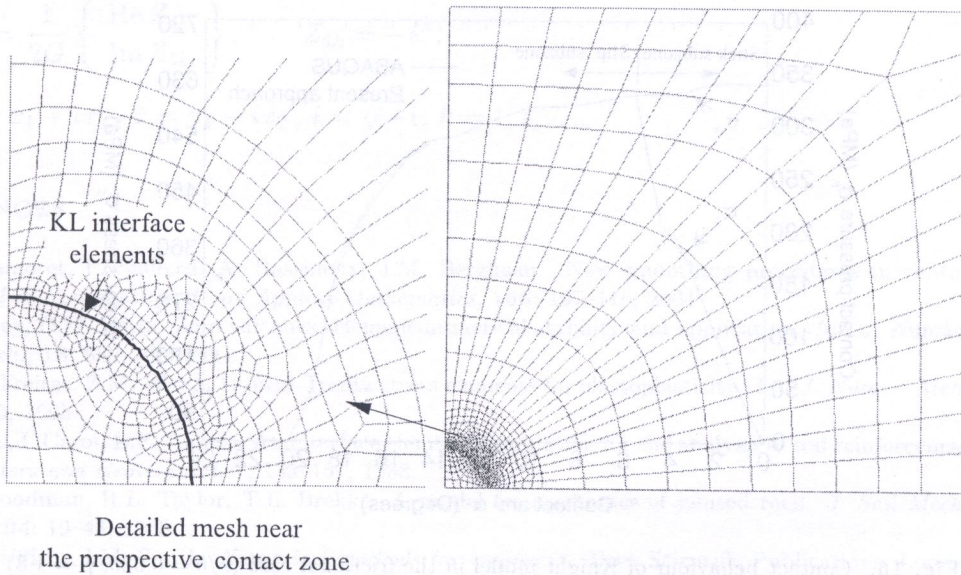


Fig. 13. Configuration of mesh for Example 2 ( $r/b = 0.083$ )

given in the literature [15, 25], the frictionless case was first considered. Based on the parametric study of Example 1,  $k_n = 2 \times 10^4 \text{ N/mm}^3$  was used in the following analysis and the corresponding mesh is shown in Fig. 13.

Figure 14 presents the results with a range of relative inclusion-matrix ratios of  $r/b = 0.5, 0.2, 0.1, 0.083$  and  $0.05$ . Numerical results presented in Fig. 14 reveal that the real contact arc and the maximum contact pressure decrease with the reduction in  $r/b$ . A stable value of  $19.62^\circ$  and  $609 \text{ MPa}$  predicted by Stippes *et al.* [25] was apparently achieved in this analysis as shown in Fig. 14. For the ratio  $r/b = 0.083$ , the results do not change substantially. In this study, the fact that the ratio of  $r/b = 0.083$  represents an infinite model shown in Fig. 12(a) accurately, which has been proved again after Knight *et al.* [15].

The results for a frictional coefficient of  $\mu = 1.8$  are presented in Fig. 15. In the HT FE-interface analysis the penalty normal and tangential stiffnesses were respectively chosen as  $k_n = 2 \times 10^4 \text{ N/mm}^3$  and  $k_\tau = 2 \times 10^3 \text{ N/mm}^3$ . Comparison of the results was made between the present model and conventional FE model (ABAQUS) and only small deviations have been found. It is also

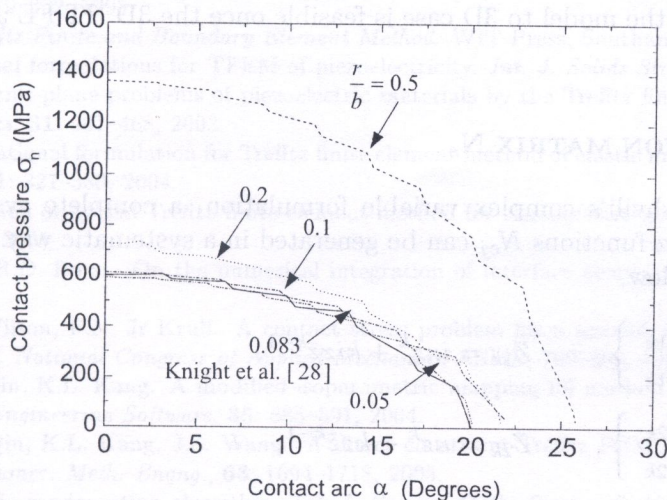


Fig. 14. Effect of  $r/b$  on the contact behaviour in the frictionless case

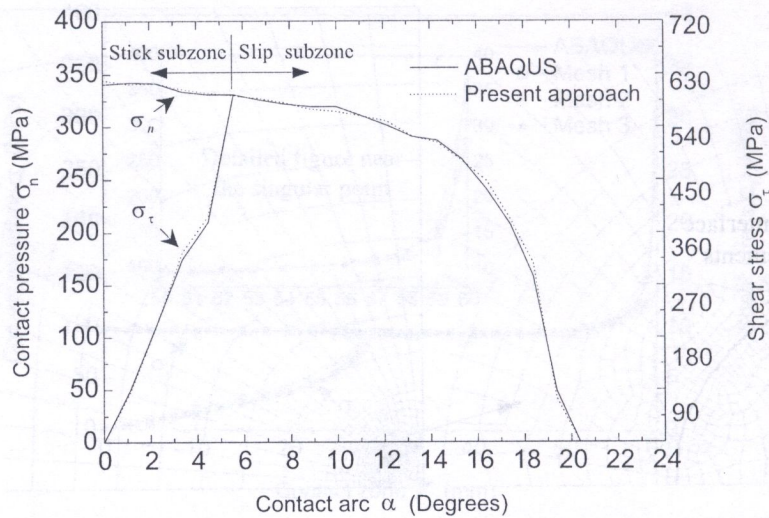


Fig. 15. Contact behaviour of Knight model in the frictional case ( $r/b = 0.083$ ,  $\mu = 1.8$ )

found that the maximum contact pressure decreases due to the influence of friction but the real contact arc remains almost identical to that in the frictionless case.

#### 4. CONCLUSIONS

An interface model for elastic contact problems using HT FEM has been developed in this paper. Four-noded HT elements were formulated and used in the discretisation of the contacting bodies whereas four-noded KL interface elements were formulated and embedded in the prospective contact zone for simulating the behaviour of interaction. In order to ensure better performance of the KL element in the analysis of contact problems, an interfacial constitutive relation, viz. normal and tangential stress vs relative displacement curves, was appropriately facilitated. Additionally, the Simpson-type Newton–Cotes integration scheme has been utilized for the KL element stiffness equation.

The HT FE-interface model was implemented in the ABAQUS (via UEL). Two benchmark examples were investigated and all computed results have proved their reliability with respect to the relevant analytical or conventional FE (ABAQUS) solutions. Especially, the effect of penalty stiffnesses on the results and the characteristic of convergence have been studied in detail.

Further extension of the model to 3D case is feasible once the 3D HT FE and interface elements are introduced.

#### A. TREFFTZ FUNCTION MATRIX $N_e$

According to Muskhelishvili's complex variable formulation, a complete system of homogeneous solutions, namely Trefftz functions  $N_{ej}$  can be generated in a systematic way. For conciseness, only the results are listed below,

$$N_{ej} = \frac{1}{2G} \begin{Bmatrix} \operatorname{Re} Z_{1k} \\ \operatorname{Im} Z_{1k} \end{Bmatrix}, \quad Z_{1k} = i\kappa z^k + kiz\bar{z}^{k-1}, \quad (1a)$$

$$N_{ej+1} = \frac{1}{2G} \begin{Bmatrix} \operatorname{Re} Z_{2k} \\ \operatorname{Im} Z_{2k} \end{Bmatrix}, \quad Z_{2k} = \kappa z^k - kzz\bar{z}^{k-1}, \quad (1b)$$

$$N_{ej+2} = \frac{1}{2G} \begin{Bmatrix} \operatorname{Re} Z_{3k} \\ \operatorname{Im} Z_{3k} \end{Bmatrix}, \quad Z_{3k} = iz^k, \quad (1c)$$

$$N_{ej+3} = \frac{1}{2G} \left\{ \begin{array}{l} \operatorname{Re} Z_{4k} \\ \operatorname{Im} Z_{4k} \end{array} \right\}, \quad Z_{4k} = -\bar{z}^k, \quad (1d)$$

where  $z = x_1 + ix_2$ ,  $\bar{z} = x_1 - ix_2$ ,  $i = \sqrt{-1}$ ,  $k = 1, 2, \dots$

## REFERENCES

- [1] D. Chamoret, P. Saillard, A. Rassineux, J.M. Bergheau. New smoothing procedures in contact mechanics. *Journal of Computational and Applied Mathematics*, **168**: 107–116, 2004.
- [2] R.A. Day, D.M. Potts. Zero thickness element-numerical stability and application. *Int. J. Numer. Meth. Anal. Geomech.*, **18**: 689–708, 1994.
- [3] J.A.T. Freitas, Z.M. Wang. Hybrid-Trefftz stress elements for elastoplasticity. *Int. J. Numer. Meth. Engng.*, **43**: 655–683, 1998.
- [4] A. Gens, I. Carol, E.E. Alonso. An interface element formulation for the analysis of soil reinforcement interaction. *Computers and Geotechnics*, **7**: 133–151, 1988.
- [5] R.E. Goodman, R.L. Taylor, T.L. Brekke. A model for mechanics of jointed rock. *J. Soil Mech., Foundation ASCE*, **94**: 19–43, 1968.
- [6] D.V. Griffiths, I.M. Smith. *Numerical methods for engineers*. Black Scientific Publications, London, 1991.
- [7] L.R. Herrmann. Finite element analysis of contact problems. *J. Eng. Mech. ASCE*, **104**: 1043–1059, 1978.
- [8] Ch. Hochard. A Trefftz approach to computational mechanics. *Int. J. Numer. Meth. Engng.*, **56**: 2367–2386, 2003.
- [9] J. Jirousek, L. Guex. The hybrid-Trefftz finite element model and its application to plate bending. *Int. J. Num. Meth. Engng.*, **23**: 651–693, 1986.
- [10] J. Jirousek, N. Leon. A powerful finite element for plate bending. *Comput. Methods Appl. Mech. Eng.*, **12**: 77–96, 1977.
- [11] J. Jirousek, Q.H. Qin. Application of hybrid-Trefftz element approach to transient heat conduction analysis. *Comput. Struct.*, **58**: 195–201, 1996.
- [12] J. Jirousek, P. Teodorescu. Large finite element method for the solution of problems in the theory of elasticity. *Comput. Struct.*, **15**: 575–587, 1982.
- [13] J. Jirousek, A. Venkatesh. Hybrid Trefftz plane elasticity elements with  $p$ -method capabilities. *Int. J. Numer. Meth. Engng.*, **35**: 1443–1472, 1992.
- [14] V.N. Kaliakin, J. Li. Insight into deficiencies associated with commonly used zero-thickness interface elements. *Computers and Geotechnics*, **17**: 225–252, 1995.
- [15] M.G. Knight, L.A. Lacerda, L.C. Wrobel, J.L. Henshall. Parametric study of the contact stresses around spherical and cylindrical inclusions. *Computational Materials Science*, **25**: 115–121, 2002.
- [16] X.Y. Lei. Contact friction analysis with a simple interface element. *Comput. Methods Appl. Mech. Engng.*, **190**: 1955–1965, 2001.
- [17] A. Pantano, R.C. Averill. A penalty-based finite element interface technology. *Comput. Struct.*, **80**: 1725–1748, 2002.
- [18] Q.H. Qin. Hybrid-Trefftz finite element method for Reissner plates on an elastic foundation. *Comp. Meth. Appl. Mech. Eng.*, **122**: 379–392, 1995.
- [19] Q.H. Qin. *The Trefftz Finite and Boundary Element Method*. WIT Press, Southampton, 2000.
- [20] Q.H. Qin. Variational formulations for TFEM of piezoelectricity. *Int. J. Solids Struct.*, **40**: 6335–6346, 2003.
- [21] Q.H. Qin. Solving anti-plane problems of piezoelectric materials by the Trefftz finite element approach. *Computational Mechanics*, **31**: 461–468, 2003.
- [22] Q.H. Qin. Dual variational formulation for Trefftz finite element method of elastic materials. *Mechanics Research Communications*, **31**: 321–330, 2004.
- [23] Q.H. Qin. Formulation of hybrid Trefftz finite element method for elastoplasticity. *Applied Mathematical Modelling*, **29**: 235–252, 2005.
- [24] J.C.J. Schellekens, R.D. Borst. On the numerical integration of interface elements. *Int. J. Solids Struct.*, **36**: 43–66, 1993.
- [25] M. Stippes, H.B. Wilson, F.N. Jr Krull. A contact stress problem for a smooth disk in an infinite plate. In: *Proceedings 4th U.S. National Congress of Applied Mechanics*, ASME, 799–806, 1962.
- [26] K.Y. Wang, Q.H. Qin, K.L. Kang. A modified isoparametric mapping fill method to display color mapping of data. *Advances in Engineering Software*, **35**: 585–591, 2004.
- [27] K.Y. Wang, Q.H. Qin, K.L. Kang, J.S. Wang. A dual constraint-Trefftz FEM for analyzing elastic contact problems. *Int. J. Numer. Meth. Engng.*, **63**: 1694–1718, 2005.
- [28] E. Wilson. The static condensation algorithm. *Int. J. Numer. Meth. Engng.*, **8**: 199–203, 1974.